의학박사 학위논문

EGFR 발현 두경부암 이식 생쥐 모델에서 ^{177}Lu 표지 항EGFR 단일클론 항체를 이용한 방사면역치료 효과에 대한 연구

Anti-tumor effect of radioimmunotherapy using ^{177}Lu-labeled anti-EGFR monoclonal antibody in head and neck squamous cell carcinoma xenograft model

2016년 8월

서울대학교 대학원

의학과 이비인후과학 전공

최 익 준

EGFR 발현 두경부암 이식 생쥐 모델에서 ^{177}Lu 표지 항EGFR 단일클론 항체를 이용한 방사면역치료 효과에 대한 연구

지도교수 이 철 희

이 논문을 의학 박사 학위논문으로 제출함

2016년 4월

서울대학교 대학원

의학과 이비인후과학 전공

최 익 준

최익준의 의학박사 학위논문을 인준함

2016년 8월

위원장	이 재 서	(인)
부위원장	이 철 희	(인)
위원	김 철 호	(인)
위원	우 홍 균	(인)
위원	천 기 정	(인)

Anti-tumor effect of radioimmunotherapy using ^{177}Lu-labeled anti-EGFR monoclonal antibody in head and neck squamous cell carcinoma xenograft model

by

Ik Joon Choi

A Thesis Submitted in Partial Fulfillment of the
Requirements for the Degree of Doctor of Philosophy
in Medicine (Otorhinolaryngology)
at the Seoul National University College of Medicine

July, 2016

Approved by thesis committee:

Chairman	Chae-Seo Rhee
Vice chairman	Chul Hee Lee
Member	Chul-Ho Kim
Member	Hong-Gyun Wu
Member	Gi Jeong Cheon

Abstract

Anti-tumor effect of radioimmunotherapy using ^{177}Lu-labeled anti-EGFR monoclonal antibody in head and neck squamous cell carcinoma xenograft model

Ik Joon Choi, M.D.
Department of otorhinolaryngology
The Graduate School
Seoul National University

Background: Epidermal growth factor receptor (EGFR) has been one of the most comprehensively studied molecular targets in head and neck squamous cell carcinoma (HNSCC). However, as monotherapy, the use of monoclonal antibodies against EGFR have shown limited efficacy. In this study, we evaluated the feasibility of EGFR-targeted radioimmunotherapy using a ^{177}Lu-labeled anti-EGFR monoclonal antibody in a SNU-1066 HNSCC mouse model.

Methods:

1. *Radiolabelling of ^{177}Lu and PCTA-cetuximab immunoconjugate*

Immunoconjugates were prepared by incubating cetuximab (20 mg)

with the bifunctional chelator, 3,6,9,15-tetraazabicyclo[9.3.1]pentadeca-1(15),11,13-triene-4-S-(4-isothiocyanatobenzyl)-3,6,9-triacetic acid (*p*-SCN-Bn-PCTA, Macrocyclics Inc., Dallas, TX, USA) (10 equivalents) in 100 mM sodium bicarbonate buffer (pH 8.5) at 4°C for overnight. Five hundred micrograms (250 μL) of immunoconjugate were reacted with ^{177}Lu solution (37~370 MBq, 0.1 M sodium acetate buffer pH 6.5) for 60 min at room temperature or 37°C, with constant shaking.

2. *Biodistribution study and Micro-SPECT/CT imaging*

SNU-1066 cells (1.2×10^7 cells) were subcutaneously injected into the right flank of 6-week-old female athymic mice. Biodistribution experiments were performed when tumor volume reached 100-300 mm^3. Mice bearing SNU-1066 HNSCC tumors were intravenously injected with a 3.7 MBq dose of ^{177}Lu-PCTA-cetuximab (n = 4) and mice were sacrificed at 14 days.

Micro-SPECT/CT was performed on the 5th day after ^{177}Lu-PCTA-cetuximab injection (12.95 MBq) in the SNU-1066 tumor model. At 30 min prior to ^{177}Lu-PCTA-cetuximab injection, excess cold cetuximab (40 mg/kg mouse body weight) was intravenously injected in a blocking experiment.

3. *Radioimmunotherapy using ^{177}Lu-PCTA-cetuximab*

SNU-1066 cells (1.2×10^7 cells in PBS pH 7.4) were subcutaneously injected into the right flank of mice. SNU-1066 tumor-bearing mice were randomly divided into four groups when tumor volume reached 100-200 mm^3 (n = 9 or 10 per group). HNSCC tumor mice model were intravenously administrated with saline, cetuximab (5 mg/kg, single dose or 10 mg/kg, three times a week for 2 weeks) or ^{177}Lu-PCTA-cetuximab (12.95 MBq, single dose), respectively. Tumor volume was calculated by (long diameter × short diameter^2) / 2 and body weight was measured three times a week.

Results:

1. *Radiolabelling of ^{177}Lu and PCTA-cetuximab immunoconjugate*

The average number of chelates per cetuximab was determined to be 4.0 ± 0.4 by MALDI mass spectrometry. ^{177}Lu-PCTA-cetxuximab was prepared successfully with high radiolabeling yield and radiochemical purity (≥ 98%) which was confirmed by Instant Thin Layer Chromatography-silica gel (ITLC-sg).

2. *Biodistribution study and Micro-SPECT/CT imaging*

The activity of ^{177}Lu decreased over time in all organs except for the SNU-1066 tumor, which continued to accumulate radioactivity up to 7 days after administration. The maximum tumor uptake was 20.6 ±

5.2%ID/g on day 7 and then decreased gradually to 17.5 ± 4.9 %ID/g on day 14. The radioactivity in blood was 29.0 ± 3.6 %ID/g at 2 h, followed by relatively fast clearance by the end of 14 days (2.3 ± 0.4 %ID/g). The %ID/g of ^{177}Lu-PCTA-cetuximab for all normal organs was always less than 10%, except for blood, liver and spleen.

3. *Radioimmunotherapy using ^{177}Lu-PCTA-cetuximab*

Treatment with a single-dose injection (12.95 MBq) of ^{177}Lu-PCTA-cetuximab treatment showed marked regression of tumor volume. ^{177}Lu-PCTA-cetuximab-treated SNU-1066 tumors on day 42 post-treatment showed a 70.3% reduction compared with that on day 2 after treatment. SNU-1066 tumor volume in the ^{177}Lu-PCTA-cetuximab-treated group showed a statistically significant difference compared to the saline-treated groups by day 9 ($P < 0.05$), the single-dose cetuximab group by day 21 ($P < 0.05$) and the multiple-dose cetuximab group by day 35 ($P < 0.05$).

Conclusion: Our results suggest that cetuximab can function as an effective carrier for tumor-targeted delivery of radiation, and that radioimmunotherapy using ^{177}Lu-PCTA-cetuximab is promising for the targeted therapy of EGFR-positive tumors compared to antibody-based immunotherapy.

Keywords: radioimmunotherapy, radioisotope, monoclonal antibody, epidermal growth factor receptor, head and neck, squamous cell carcinoma

Student Number: 2010-31149

Contents

List of Table

List of Figures

Introduction

Head and neck squamous cell carcinoma (HNSCC) is the sixth leading cancer by incidence worldwide with more than 500,000 new cases per year. Patients with HNSCC are treated with surgery, radiotherapy alone, or surgery combined with postoperative adjuvant radiotherapy or chemotherapy.[1] Recently, concomitant chemoradiation has become increasingly popular for advanced resectable cancers, although there seems to be no survival advantage when compared with other forms of therapy.[2-4] There is thus an urgent need for both early detection of HNSCC and development of new therapeutic regimens and drugs.

The epidermal growth factor receptor (EGFR) is a transmembrane tyrosine kinase protein overexpressed in the majority of epithelial malignancies.[5] It belongs to the ErbB family of receptor tyrosine kinases which also includes ErbB2 (HER-2 or Neu), ErbB3 (HER-3) and ErbB4 (HER-4).[6] Overexpression of EGFR mRNA or protein is found in approximately 90% and 40% of HNSCC cases, respectively,[7–9] and this overexpression is associated with poor prognosis, increased tumor growth, metastasis and resistance to chemotherapy and radiation therapy.[10] In the past decades, the EGFR has been one of the most comprehensively studied molecular targets in oncology therapeutics.

Despite the enthusiasm and optimism accompanying the development of agents targeting EGFR, only a minority of patients have benefitted from these drugs. As a monotherapy, small-molecule tyrosine kinase inhibitors (gefitinib and erlotinib)[11,12] and monoclonal antibodies (mAbs) against EGFR (cetuximab, panitumumab, and zalutumumab) have shown limited efficacy.[13]

Cetuximab is the most studied targeted therapy for HNSCC. It is a chimeric human: murine immunoglobulin (Ig) G1 mAb that binds to EGFR with an affinity similar to that for its natural ligands, epidermal growth factor (EGF) and transforming growth factor-a (TGF-a), thus preventing activation of downstream signaling pathways. In addition, it induces antibody-dependent cellular cytotoxicity, inhibits nuclear EGFR transport and suppresses the DNA-dependent protein kinase.[14–16]

In contrast to "naked" antibody-based immunotherapy, other strategies have also been extensively investigated for cancer therapy. For example, antibodies can function as carriers for cancer-targeted specific delivery of cytotoxic substances (such as radioisotopes, drugs, and toxins). The resulting immunoconjugates have shown promising results for cancer therapy. In the case of radioimmunoconjugates (antibodies labeled with radioisotopes), both pre-clinical and clinical studies have demonstrated greater effectiveness compared with immunotherapy with unconjugated antibodies.[19-22] Radioimmunotherapy (RIT) offers the opportunity to

selectively kill tumor cells while sparing normal tissues, and not every tumor cell must be targeted by antibodies. Instead, tumor cells can be destroyed by the "cross-fire" effect. ^{177}Lu is a low-energy β− emitter with both β and γ emissions. The low β− energy can be used for radionuclide therapy, while the presence of γ emission permits single-photon emission computed tomography (SPECT) imaging for quantification of biodistribution and determination of radiation dosimetry. [23, 24]

In this study, we evaluated the *in vitro* and *in vivo* EGFR-targeting properties of a ^{177}Lu -labeled anti-EGFR antibody (cetuximab) in a SNU-1066 HNSCC mouse model and demonstrated the feasibility of EGFR targeted radioimmunotherapy for EGFR-positive tumors compared to antibody-based immunotherapy.

Materials and Methods

Cell culture

Human head and neck squamous cell carcinoma, YD-8, SNU-1041, SNU-1066 and SNU-1076 cells were purchased from Korea Cell Line Bank (Seoul, South Korea). YD-8, SNU-1041, SNU-1066 and SNU-1076 cells were grown in RPMI (Invitrogen, Carlsbad, CA, USA) containing 10% fetal bovine serum (FBS; Hyclone) (GE Healthcare Life Sciences, Chicago, IL, USA) in a 5% CO_2, 37°C humidified incubator.

Total RNA isolation and RT-PCR

RNA was extracted using the RNeasy Mini kit (Qiagen, Hilden, Germany). cDNA was produced by reverse transcription of 1 μg total RNA using oligo-dT primers and SuperScript II reverse transcriptase (Invitrogen, California, USA). cDNA was amplified with EGFR (Fwd: 5'-GTCCTCCATCTCATAGCTG-3', and Rev: 5'-GAGAGGAGAACTGCCAGAAA-3') primers. The PCR products were then degraded by electrophoresis using 2% agarose gels. GAPDH (Fwd: 5'-GTC AGT GGT GGA CCT GAC CT-3', Rev: 5'-TGC TGT AGC CAA ATT CGT TG-3') was used as a control.

Western blot analysis

HNSCC cells (YD-8, SNU-1041, SNU-1066, SNU-1076) were lysed in RIPA buffer (Thermo Scientific, Rockford, IL, USA) containing protease inhibitors (GenDEPOT, Katy, USA) for protein extraction. Western blot was performed according to standard protocols (Bio-RAD Laboratories, Inc., Hercules, CA, USA). Protein lysates (25 μg) were separated using 10% SDS-polyacrylamide gels and, transferred to nitrocellulose blotting membranes (GE Healthcare Life Sciences, Chicago, IL, USA). After gel transfer, the membrane was incubated with blocking solution and agitated for 1h at a room temperature and then probed with anti-EGFR primary (Santa Cruz Biotechnology, Santa Cruz, CA, USA) and appropriate secondary antibodies. After three additional washes in TBST, specific proteins were detected using a chemiluminescence detection system. β-actin (Sigma Aldrich, St. Louis, MO, USA) was used as a loading control.

Flow cytometry

HNSCC cells were harvested and washed with PBS containing 3% bovine serum albumin. The cells were incubated with cetuximab (5mg/ml: 2 μl) for 1h. The control cell group was incubated with

rituximab (10mg/ml: 1 µl) for 1h. After the washes, monoclonal anti-human FITC-conjugated IgG antibody (1-2 mg/ml, 1 µl, Sigma F501) was added to cells and incubated for 1 h at 4°C. After the cells were washed three times with PBS, they were fixed with 4% paraformaldehyde and analyzed using FACSCalibur (Becton Dickinson Biosciences, Franklin Lakes, NJ, USA) to detect the intensity of EGFR expression at the cell surface.

Cell viability assay

Cell viability was determined using MTS assay. Cells were seeded in 96-well-plates at a 4×10^3cells/well in culture media and incubated for 24h. After this, the media was removed and cells were treated with different doses of cetuximab (0, 1, 10, 50, 100, 200, and 500 µg /ml) for either 72, 120, or 168h. The cells were then incubated with Celltiter 96 AQueous One (MTS) solution (Promega, Madison, WI, USA) for 1h. Absorbance was measured at 490nm using a microplate reader (Biotek, Winooski, VT, USA).

Preparation of PCTA-cetuximab immunoconjugate

Immunoconjugates were prepared by incubating cetuximab (20 mg) with the bifunctional chelator, 3,6,9,15-

tetraazabicyclo[9.3.1]pentadeca-1(15),11,13-triene-4-S-(4-isothiocyanatobenzyl)-3,6,9-triacetic acid (*p*-SCN-Bn-PCTA, Macrocyclics Inc., Dallas, TX, USA) (10 equivalents) in 100 mM sodium bicarbonate buffer (pH 8.5) at 4°C overnight. Unreacted bifunctional chelate was removed using a 10 kDa MW cut-off dialysis cassette (Thermo Scientific) with 10 mM sodium acetate buffer (pH 6.5). The immunoconjugates were concentrated using centrifugtion device to 2 mg/mL and stored at 4°C. The amount of chelate per antibody was determined after purification. Antibody concentration was determined by UV 280 nm absorbance. Matrix-assisted laser desorption ionization (MALDI) mass spectra of cetuximab and PCTA-conjugated cetuximab were analyzed by a MALDI mass spectrophotometer (Voyager-DE STR, PerSpective Biosystyems, Inc., Ohchang, South Korea).

Radiolabeling

$^{177}LuCl_3$ was purchased from ITG AG (Zug, Switzerland). Five hundred micrograms (250 μl) of immunoconjugate was reacted with ^{177}Lu solution (37-370 MBq, 0.1 M sodium acetate buffer pH 6.5) for 60 min at room temperature or 37°C with constant shaking. Radiolabeling yield and radiochemical purity were analyzed by Instant

Thin Layer Chromatography-silica gel (ITLC-sg) as a stationary phase and 20 mM citrate buffer with 50 mM EDTA (pH 5.0) as a mobile phase.

Cell binding assay

To evaluate the immunoreactivity of ^{177}Lu-radiolabeled cetuximab towards EGFR, as well as EGFR expression levels in HNSCC cell lines, an *in vitro* cell binding assay was performed. Cell binding studies evaluating ^{177}Lu-PCTA-cetuximab were performed using HNSCC cell lines, YD-8, SNU-1041, SNU-1066 and SNU-1076; 1×10^6 cells were used per test tube. In the non-specific binding experiment, cetuximab antibody (10 μg) was pre-incubated for 1 h at 4°C. ^{177}Lu-PCTA-cetuximab (100 ng) was added to all test tubes. After 60 min incubation at 4°C, cell pellets were triple washed in cold PBS with 1% BSA and counted with a gamma counter (Wizard 1480, Perkin-Elmer, Waltham, MA, USA). Cell bound radioactivity (%) was measured and expressed as the percentage of added radioactivity dose.

Cytotoxicity assay of ^{177}Lu -PCTA-cetuximab

SNU-1066 cells were seeded in 6-well plates at 5×10^4 cells/well and incubated for 18 h. The cells were treated with ^{177}Lu-PCTA-cetuximab

at 0.037, 0.37, 0.74 and 1.48 MBq/well in culture media containing 1% FBS. Corresponding control wells were treated with media alone and unlabeled cetuximab in equal concentrations (2 μg/well) to radiolabeled antibody. After 1 h incubation, the treated media was aspirated and fresh media was added to each well. On days 3, 4, and 5 after treatment, the cytotoxic effects of ^{177}Lu-PCTA-cetuximab were evaluated by determining cell viability using an automated cell counter (ADAM-MC, Digital-Bio, Seoul, South Korea). Data were expressed as the percentage of control proliferation using the number of living cells incubated with media alone as a control. We examined the effects of ^{177}Lu-PCTA-cetuximab on EGFR and downstream signaling pathways mediated by Akt or Erk in SNU-1066 cells.

Biodistribution study

All animal studies were conducted in accordance with guidelines of the Institutional Animal Care and Use committee (IACUC) at the Korea Institute of Radiological and Medical Sciences (KIRAMS). Female athymic mice (6 weeks) were obtained from Nara Biotech (Seoul, South Korea). SNU-1066 cells (1.2×10^7 cells) were subcutaneously injected into the right flank of mice. When tumor volume reached 100-300 mm^3, biodistribution experiments were performed. Mice bearing

SNU-1066 HNSCC tumors were intravenously injected with a 3.7 MBq dose of ^{177}Lu-PCTA-cetuximab (n = 4) and sacrificed 14 days later. For the blocking experiment, tumor-bearing mice were pre-injected with 40 mg/kg of cetuximab 2 h prior. Blood and normal tissues were collected and SNU-1066 tumors were also excised. All samples were weighed, and sample radioactivity was measured using a NaI crystal well-type gamma counter applying a decay correction. Counts were compared with those of standards, and the data were expressed as the percentage of injected dose per gram of tissue (%ID/g).

Radiation dosimetry

Estimated human dosimetry was calculated from the biodistribution results from SNU-1066 tumor-bearing mice injected with about 3.7 MBq of ^{177}Lu-PCTA-cetuximab. Time-activity curves were generated from the mean values obtained in mice for each tissue of interest. We then calculated source organ residence times for the human model by integrating a mono-exponential fit to the experimental biodistribution data for the major organs and the whole body. Murine normal organ cumulated activities were converted to human normal organ cumulated activities by adjusting for the differences in total-body and organ masses between mice and humans (assuming a 70-kg standard human).

The calculated human normal organ cumulated activities were entered into the Organ Level Internal Dose Assessment (OLINDA, Vanderbilt University, Nashville, TN, USA) dosimetry computer program v1.0 to calculate, using the formulae of the Medical Internal Dosimetry Committee of the Society of Nuclear Medicine,[39] the standard human organ absorbed doses. Extrapolated radiation dosimetry for humans was prepared by assuming that the metabolism rates and pharmacokinetics of ^{177}Lu-PCTA-cetuximab in man and mouse are equivalent.

Micro-SPECT/CT imaging

Micro-SPECT/CT was performed on the 5th day after injection of ^{177}Lu-PCTA-cetuximab (12.95 MBq) in the SNU-1066 tumor model. At 30 min prior to ^{177}Lu-PCTA-cetuximab injection, excess cold cetuximab (40 mg/kg mouse body weight) was intravenously injected for a blocking experiment. Whole body mouse imaging was performed using a NanoSPECT/CT tomograph (Bioscan, Poway, CA, USA) equipped with 4 NaI detectors and fitted with 1.4-mm mouse whole body multipinhole collimators with 9 pinholes (full width at half maximum $\leq$ 1.2 mm). A total of 24 projections were acquired in a 256 $\times$ 256 acquisition matrix with 200 s per projection. Images were

reconstructed using a 2D ordered-subset expectation maximization algorithm (9 iterations). Cone-beam CT images were acquired (180 projections, 1 s/projection, 45 kVp, 177 μA) before micro-SPECT imaging. Co-registration of micro-SPECT and CT images was performed using InVivoScope software (ver. 2.0, Bioscan). After SPECT/CT scanning, mice were immediately euthanized, and frozen, and digital whole body autoradiography (DWBA) was performed.

Radioimmunotherapy

SNU-1066 cells (1.2×10^7 cells in PBS pH 7.4) were subcutaneously injected into the right flank of mice. When tumor volume reached 100 - 200 mm^3, SNU-1066 tumor-bearing mice were randomly divided into four groups (n = 9 or 10 per group). HNSCC tumor mice were intravenously administrated with saline (control group), cetuximab (5 mg/kg single dose [single dose group] or 10 mg/kg, three times a week for 2 weeks [multiple dose group]), or ^{177}Lu-PCTA-cetuximab (12.95 MBq single dose) respectively. Tumor volume was calculated by (long diameter × short diameter^2 / 2 and body weight was measured three times a week.

Therapeutic response monitoring by ^{18}F-FDG-PET imaging

To assess tumor response to ^{177}Lu-PCTA-cetuximab therapy, ^{18}F-FDG-positron emission tomography (PET) imaging was performed before treatment and at 1, 2 and 4 weeks after treatment.

Immunohistochemistry and TUNEL assay in SNU-1066 tumors. Tumor tissues were harvested on day 16 post-treatment and immediately fixed in 4% paraformaldehyde. Apoptosis was detected using a terminal deoxynucleotidyl transferase dUTP nick end-labeling (TUNEL) assay kit (Millipore, Darmstadt, Germany) on 4-μm-thick sections according to the manufacturer's instructions. Tumor sections were stained with a Ki-67 specific SP6 rabbit mAb (Abcam, Cambridge, UK), and the EnVision 1 detection system for rabbit antibody (Dako, Glostrup, Denmark) was applied according to the manufacturers' instructions. Counterstaining was performed with Mayer's hematoxylin. Nuclear staining of Ki-67 was considered positive. TUNEL-positive nuclei were counted in 6 random fields and the Ki-67 staining index was defined as the percentage of positive nuclei per 800 –1,000 nuclei.

Statistical analysis

Quantitative data are represented as the mean ± SD and statistical analysis was performed by one-way ANOVA or Student's t test using

Prism 5 (GraphPad Software, La Jolla, CA, USA). *P* values of < 0.05 were considered statistically significant.

Results

EGFR expression and cell binding assay and cytotoxicity assay of ^{177}Lu-PCTA-cetuximab in HNSCC cell lines

The relative expression levels of EGFR in four HNSCC cell lines were determined by Western blotting (Figure 1A) and flow cytometry (Figure 1B). Median fluorescence intensities were 33.4 for YD-8, 97.3 for SNU-1041, 112.4 for SNU-1066, and 91.4 for SNU-1076. As determined by flow cytometry and Western blotting, SNU-1066 cells expressed relatively higher level of EGFR expression than YD-8, SNU-1041 and SNU-1076 cells. The anti-growth effect of cetuximab was determined using SNU-1066 cells exposed to different concentrations from day 3 to day 7 after treatment (Figure 1C). The viability of SNU-1066 cells treated with cetuximab decreased in a dose-dependent manner, as evaluated by a MTS assay. EGFR expression levels obtained from flow cytometry and Western blotting was compared with results from a cell binding assay, performed using ^{177}Lu-PCTA-cetuximab. Cell bound radioactivity (%) of ^{177}Lu-PCTA-cetuximab in HNSCC cell lines was 76.3±0.8% in SNU-1066, 65.5±2.0% in SNU-1076, 47.8±1.5% in SNU-1041 and 26.9±0.8 % in YD-8 (Figure 2A). Cell viability after treatment with varied radioactivity doses of ^{177}Lu -

PCTA-cetuximab is presented in Figure 2B. At a dose of 1.48 MBq, the percentage of surviving cells decreased to 25.3 ± 1.2% by day 5 after treatment. ^{177}Lu-PCTA-cetuximab showed a radioactivity dose-dependent and time-dependent increase in cytotoxicity, which was the most significant at the 1.48 MBq/well relative to the untreated control ($P < 0.001$). Activation of EGFR signaling pathways by ^{177}Lu-PCTA-cetuximab presented a decrease in phosphorylated Akt (p-Akt) and phosphorylated Erk (p-Erk) in time-dependent manner, without affecting the total amounts of EGFR, Akt, and Erk (Figure 2C).

Characteristics of ^{177}Lu-PCTA-cetuximab

The average number of chelates per cetuximab was determined to be 4.0 ± 0.4 by MALDI mass spectrometry (Figure 3A). ^{177}Lu-PCTA-cetxuximab was prepared successfully with high radiolabeling yields and radiochemical purity (≥ 98%), as checked by ITLC-sg (Figure 3B).

Biodistribution of ^{177}Lu-PCTA-cetuximab in SNU-1066 tumor-bearing mice

The biodistribution data of ^{177}Lu-PCTA-cetuximab was obtained in SNU-1066 tumor-bearing mice (Table 1 and Figure 4). The activity of ^{177}Lu decreased with time in all organs except for the SNU-1066 tumor,

which continued to accumulate radioactivity up to 7 days after administration. The maximum tumor uptake was 20.6 ± 5.2%ID/g on day 7. Radioactivity then decreased gradually to 17.5 ± 4.9 %ID/g by day 14. The radioactivity in blood was 29.0 ± 3.6 %ID/g at 2 h, followed by relatively fast clearance by the end of 14 days (2.3 ± 0.4 %ID/g). The %ID/g of ^{177}Lu-PCTA-cetuximab for all normal organs was always less than 10%, except for blood, liver and spleen.

Pre-injection of a blocking dose of cetuximab markedly reduced the uptakes of ^{177}Lu-PCTA-cetuximab by SNU-1066 tumors to 34.4% at 48 h and 26.0% on days 7 after administration relative to mice injected with ^{177}Lu-PCTA-cetuximab alone.

Radiation dosimetry of ^{177}Lu-PCTA-cetuximab in SNU-1066 tumor-bearing mice

For the clinical translation of ^{177}Lu-PCTA-cetuximab as a radioimmunotherapeutic agent, human dosimetry is important. The estimated absorbed doses for the major organs and whole body obtained from the biodistribution data in SNU-1066 tumor-bearing mice are presented in Table 2. Lower large intestine, stomach, kidney, liver, lung and spleen showed relatively higher radiation absorbed doses. The whole body absorbed dose was founded to be 0.33

mGy/MBq administrated. However, the radiation dose of red marrow was relatively low

The estimated absorbed doses for SNU-1066 tumor were 6455.1±2957.1 mGy/MBq.

Micro-SPECT/CT imaging and DWBA of ^{177}Lu-PCTA-cetuximab

Micro-SPECT/CT imaging was performed to investigate the *in vivo* behavior of ^{177}Lu-PCTA-cetuximab. Representative volume images and coronal images of SNU-1066 tumor-bearing mice on the 5th day post ^{177}Lu-cetuximab injection were shown in Figure 5. The SNU-1066 tumor was clearly visualized and relatively lower uptake was also observed in the liver. DWBA images showed a similar distribution pattern as the micro-SPECT/CT images. In the blocking experiments, the tumor uptake of ^{177}Lu-PCTA-cetuximab was markedly reduced by administration of excess cold cetuximab, indicating that EGFR targeting by ^{177}Lu-PCTA-cetuximab was specific.

Radioimmunotherapy in SNU-1066 tumor-bearing mice

We investigated the *in vivo* tumor treatment efficacy of cetuximab-based immunotherapy, as well as ^{177}Lu-PCTA-cetuximab-based

radioimmunotherapy in the SNU-1066 tumor mouse model (Figure 6). A time-dependent increase in tumor volume was observed in the saline-treated group, in which the tumors presented average volumes over 700 mm3 on day 42. Treatment with a single dose of cetuximab inhibited tumor growth until day 14 post-injection, whereas treatment with multiple doses of cetuximab reduced the tumor volume until day 16. However, tumor regrowth was observed in cetuximab-treated groups, and average tumor volumes exceeded 300 mm^3 on day 42. In contrast, treatment via a single-dose injection (12.95 MBq) of ^{177}Lu-PCTA-cetuximab showed marked regression of tumor volume. ^{177}Lu-PCTA-cetuximab-treated SNU-1066 tumors on day 42 after treatment showed a 70.3% reduction relative to size at day 2 after treatment. SNU-1066 tumor volume in ^{177}Lu-PCTA-cetuximab-treated group showed a statistically significant difference compared to tumor volume in the saline-treated group by day 9, the single-dose cetuximab treatment group by day 28 and multiple-dose cetuximab treatment group by day 35 ($P < 0.05$). SNU-1066 tumor models tolerated the ^{177}Lu-PCTA-cetuximab treatment, and no apparent body weight loss was observed (Figure 7). These results suggest that the 12.95 MBq dose used in this study had no observable toxicity on mice.

Therapeutic response monitoring by ^{18}F-FDG-PET imaging

There was little difference in ^{18}F-FDG uptake of the saline-treated group for the 4 weeks of treatment. In the cetuximab (single dose) treatment group, ^{18}F-FDG standard uptake value (SUV) was reduced at 1 week after treatment. However, SUV increased by 2 weeks, and was fully restored at 4 weeks after treatment. In contrast, the ^{177}Lu-PCTA-cetuximab treatment group (0.37 ± 0.12) showed marked reduction of ^{18}F-FDG SUV compared to the saline treatment (1.00 ± 0.08) or cetuximab treatment groups (1.06 ± 0.12) at 4 weeks after treatment ($P < 0.05$) (Figure 8).

Immunohistochemistry and TUNEL assay in SNU-1066 tumors.

To determine the mechanism by which ^{177}Lu-PCTA-cetuximab inhibited tumor growth in nude mice, we measured cell proliferation and apoptosis using immunohistochemistry and TUNEL assay in excised xenografts. Cells positive for the proliferation marker Ki-67 were noticeably reduced in the ^{177}Lu-PCTA-cetuxiamb treatment group (Figure 9A). The number of Ki-67-positive cells was quantified using the ImageJ program, and significantly lower numbers of Ki-67-positive cells were found in the ^{177}Lu-PCTA-cetuximab treatment group (saline: 85.2±3.8 vs. cetuximab: 81.3±3.1 vs. ^{177}Lu-PCTA-cetuxiamb: 45.1±7.0, $P<0.01$; Figure 9C). To determine the level of apoptosis in the xenograft, we performed TUNEL assays. There were statistically

significant differences in the ^{177}Lu-PCTA-cetuximab (14.5 ± 7.0 cells per field) treatment group compared to the saline (0.7 ± 0.8) and cetuximab treatment (0.5 ± 0.5) groups ($P > 0.05$; Figure 9A and B), suggesting that the reduction of tumor size was caused by apoptosis.

Discussion

Monoclonal antibodies bound to cancer cells are capable of killing cancer cells through two basic mechanisms: immunologic and signal transduction, and in many cases both mechanisms are operative. Signal transduction mechanisms involve disrupting cellular signaling pathways that are required to sustain a tumor phenotype such as growth or apoptotic signaling modulation. Immunologic mechanisms include antibody dependent cellular cytotoxicity (ADCC) and complement dependent cytotoxicity (CDC). In solid tumors, ADCC and affinity for FcRIIIa have been found to be involved in the antitumor activity of naked monoclonal antibodies such as cetuximab.[31]

EGFR-targeted therapies include mAbs, such as cetuximab (IMC-C225, Erbitux) and panitumumab (ABX-EGF, Vectibix), which block the extracellular ligand-binding domain of the receptor, as well as tyrosine kinase inhibitors that prevent the activation of the cytoplasmic kinase portion.[27] These targeting approaches have shown great promise in preclinical studies.[28] Cetuximab is currently approved in combination with radiation therapy in locally-advanced disease[17]; as a single agent in platinum-refractory recurrent/metastatic disease,[13] and in combination with platinum (carboplatin or cisplatin) and 5-fluorouracil,

as first line therapy in recurrent/metastatic disease.[18] However, it should be noted that response rates as a single agent have been less than satisfactory (13%) and of limited duration (2–3 months). [13] Increasing clinical evidence has indicated that EGFR-positive tumors are not certain to benefit from treatment with anti- EGFR mAbs alone, although the detailed mechanism of tumor resistance still requires further investigation.

Many studies have suggested different mechanisms that may be contributing to EGFR blockage resistance, such as HER-2 amplification, phosphatidylinositol 3-kinase/Akt pathway, mesenchymal–epithelial transition factor amplification, aurora kinase, EGFR variant III, and vascular endothelial growth factor.[38]

To overcome the limits of single agent anti-EGFR-based immunotherapy, we evaluated the anti-tumor effect of a radioimmunotherapy using ^{177}Lu-labeled anti-EGFR monoclonal antibody in a HNSCC xenograft model.

Radioimmunotherapy using radiolabeled antibodies have the potential to kill cancer cells through two therapeutic components: radiation delivery and antibody action upon binding.

Radiation kills cancer cells primarily by damaging DNA.[29] When cancer cells are irradiated, both DNA single strand breaks and double strand breaks can occur. Single strand breaks are readily repaired

although sometimes point mutations can be generated. Double strand breaks are the most important lesions caused by radiation leading to chromosome aberrations that kill cells through apoptosis or mitotic death.

Both low dose rate and bystander effects of radiation have been proposed to explain the improved efficacy of radioimmunotherapy over external beam radiation at equivalent doses.[30]

In conventional radiation therapy, high radiation doses are needed to achieve clinical responses in solid tumors such as prostate cancer (64.8-81 Gy),[40] lung cancer (40-65 Gy),[41] glioma (60 Gy),[42] breast cancer (50 Gy),[43] colorectal cancer (70 Gy)[44] and pancreatic cancer (50.4 Gy).[45] Based on these clinical experiences, it is generally accepted that solid tumor doses need to reach at least 50 Gy to achieve any clinical benefits.

Unfortunately, tumor radiation doses are below 50 Gy in most reported radioimmunotherapy studies of solid tumors. In a phase I trial of 131I labeled anti-TAG72 mAb (CC49) to treat metastatic gastrointestinal cancers, tumor absorbed doses in metastatic sites ranged from 6.3 to 33 Gy.[45] In a similar study, the tumor doses for 90Y- CC49 were found to be 1.8 to 30 Gy.[46].

Our results showed that radiation doses of ^{177}Lu-PCTA-cetuximab in

SNU-1066 tumor-bearing mice was 6.5 × $10^3 \pm 3.0 \times 10^3$ mGy/MBq from the biodistribution data and 5.2× $10^3 \pm 1.1 \times 10^3$ mGy/MBq (66.2 Gy/12.95MBq) from RIT data. This radiation dose is thought be sufficient to achieve clinical benefits in the tumor while maintaining low doses exposure in other organs.

In the past decade, radiolabeled antibodies have seen tremendous success in treating non-Hodgkins' lymphoma (NHL) resulting in FDA approval of ^{90}Y ibritumomab tiuxetan (Zevalin) and ^{131}I tositumomab (Bexxar) for CD20-targeted therapy. However, radioimmunotherapy has been mainly applied in hematooncologic malignancies such as CD20-positive NHL, rather than solid tumors such as HNSCC.

EGFR has been actively investigated as a novel therapeutic target for HNSCC. EGFR is highly expressed in HNSCC and is further increased in recurrent and metastatic HNSCC. EGFR undergoes internalization constitutively by binding to a ligand. In this regard, EGFR could be an advantageous target for imaging.

Targeted radionuclide therapy using small molecules is also advantageous in various aspects. It can maximize therapeutic effects based on the biological effects of particle emitting radiation, and minimize adverse effects by means of reducing the amount of injected drugs. Besides, not only targeted tumor cells can be selectively killed,

but also non-targeted adjacent tumor cells can be destroyed via the cross-fire effect or bystander effect.

We found that EGFR is overexpressed in the SNU-1066 cancer cell line compared to other cell lines (Figure 1A, 1B) and our *in vitro* therapy study showed that mAb treatment had a significant antitumor effect on SNU-1066 cancer cells (Figure 1C). We developed ^{177}Lu-PCTA-cetuximab, radiolabeled immunoconjugates using the ^{177}Lu as radionuclide, PCTA as metal chelates and cetuximab as the anti-EGFR mAb. The most common radionuclides used for RIT of HNSCC model are ^{90}Y (yttrium) and ^{177}Lu (lutetium). These two radionuclides have their respective advantages and disadvantages because of differences in emission properties and chemical stability, which are important factors that contribute to the effectiveness of RIT. The advantages of ^{90}Y are that it delivers higher beta-energy to the tumor (2.3 MeV versus 0.61 MeV for ^{177}Lu) and has a longer mean path length over which 90% of the emitted energy is absorbed. (5.3mm versus 0.8mm for ^{177}Lu). These characteristics improve the ability of a radiolabeled antibody to kill both targeted and neighboring cells, which is particularly important when faced with bulky or poorly vascularized tumors. In addition, because of ^{90}Y is a pure beta-emitting radioisotope, no hospitalization, isolation, or shielding is required, and patients can receive treatment as outpatients. However, ^{90}Y is very expensive, and cannot be used for

imaging since it does not emit gamma rays.[33, 34] Compared with ^{90}Y, the advantages of ^{177}Lu are that ^{177}Lu is commercially available, is easily conjugated to antibodies, and has a long history of safe medical use. In addition, ^{177}Lu can be used for imaging because it emits gamma-energy. However, usage of ^{177}Lu requires hospitalization with shielding, and can irradiate distant organs.[23, 24] Given this, we, with consideration towards potential clinical application, chose ^{177}Lu as the radioisotope for this study.

To attach a metal radioisotope to a targeting molecule a bi-functional chelate (BFC) is typically required. Currently available BFCs are limited by either their radiolabeling chemistry or physiological stability. 3,6,9,15-tetraazabicyclo[9.3.1]pentadeca-1(15),11,13-triene-3,5,9-triacetic acid (PCTA) possessed superior reaction kinetics relative to 1,4,7,10-tetraazacyclododecane-1,4,7,10-tetraacetic acid (DOTA) under all radiolabeling conditions. For ^{177} Lu, >98% radiochemical yields were achieved in <5 min at room temperature even when using stoichiometric amounts of BFC. PCTA is efficiently labeled at a pH as low as 2 and as high as 9 and clearance of the label from the kidneys of the animals was faster with ^{64}Cu-PCTA than with ^{64}Cu-DOTA. [35]

Our data showed that ^{177}Lu-PCTA-cetxuximab was successfully prepared with high radiolabeling yield and radiochemical purity (≥

98%), as confirmed by ITLC-sg (Figure 3).

The therapeutic efficacy of RIT relies on the radiation dosimetry delivered to the tumor, and higher tumor uptake of a RIT agent is expected to cause greater anti-tumor effect. Therefore, the therapeutic efficacy of RIT can be predicted by determining the tumor uptake of the RIT agent via PET or SPECT imaging.

Our small-animal SPECT/CT imaging and biodistribution studies demonstrated that both mAbs labeled with ^{177}Lu localized to the tumor with high contrast compared to other organs except for the liver due to the hepatic clearance of antibodies (Figures 4 and 5). EGFR specificity was also confirmed by a blocking study, which is consistent with previous studies.[7,28] Given the high antibody tumor accumulation observed, we speculated that ^{177}Lu-PCTA-cetuximab could be used for EGFR-targeted RIT. We applied a single dose of 12.95 MBq of ^{177}Lu-PCTA-cetuximab for RIT of SNU1066 tumors in this study. No evident weight loss was observed after ^{177}Lu-PCTA-cetuximab (Figure 7), indicating that 12.95 MBq of ^{177}Lu-PCTA-cetuximab was below the maximum tolerated dose of the animals. RIT significantly inhibited tumor growth in the ^{177}Lu-PCTA-cetuximab treatment group (Figure 6). ^{177}Lu-PCTA-cetuximab-treated SNU-1066 tumor on day 42 after treatment presented a 70.3% size reduction relative to day 2 after treatment. A single dose of ~ 100 μg of antibody was used for RIT,

which is much lower than the dosage used for immunotherapy (multiple dose group: 200 μg, 6 times /2 weeks) and the same dosage used for unconjugated mAbs (single dose group). Thus, we believe that the therapeutic effect of ^{177}Lu-PCTA-cetuximab was due to the radiation dose delivered by cetuximab, and not by the immunotherapeutic effect of mAbs.

In contrast to the repeated injection of large amounts of naked antibodies, therapy with radiolabeled antibodies could be administered using small quantities in a single or fractionated dosing schedule. As such, we expect that complications, such as skin rash and desquamation, resulting from anti-EGFR mAb immunotherapy could be reduced.

In the present study, we evaluated whether cetuximab can function as an effective carrier for the tumor-targeted delivery of radiation in a xenograft mouse model. We found that the delivery of the EGFR-targeted mAb could be visualized by PET/CT imaging with ^{64}Cu-PCTA-cetuximab in a xenograft model (data not presented). This is one of the virtues of radioisotope-labeled mAbs, since they can be labeled with imaging radioisotopes as well. ^{64}Cu-PCTA-cetuximab possesses the same chemical and biological characteristics as the therapeutic ^{177}Lu-PCTA-cetuximab. Thus, both radionuclides would be easily interchangeable, indicating that radionuclide-labeled anti-EGFR mAbs are useful and versatile.

These data suggested that although no correlation with tumor EGFR expression was observed, quantitative PET imaging with radiolabeled antibodies enables visualization and quantification of a number of parameters, including tumor-specific binding, perfusion, vascularity, vascular permeability, and plasma half-life, and could provide more comprehensive information about antibody delivery than immunohistochemistry or fluorescence *in situ* hybridization.[36]

The internalization of ^{177}Lu-PCTA-cetuximab was also verified by autoradiography and SPECT/CT. Autoradiographic images showed strong expression in tumors xenografted with EGFR positive cells, and suggested that the ^{177}Lu-PCTA-cetuximab presented along the cell membrane of the tumor. We could identify the internalization of ^{177}Lu-PCTA-cetuximab in a xenograft model using DWBA (Figure 5D) at 5 days post-injection of ^{177}Lu-PCTA-cetuximab (12.95 MBq /100 μg/0.1 mL). FDG-PET/CT imaging SUVs obtained pre-treatment (0.90 ± 0.01 vs. 0.94 ± 0.14 vs. 0.94 ± 0.05; P = 0.89), as well as at 1 (0.74 ± 0.01 vs. 0.69 ± 0.09 vs. 0.90 ± 0.18; P = 0.69) and 2 weeks (0.63 ± 0.15 vs. 0.86 ± 0.08 vs. 1.00 ± 0.07; P = 0.105) post-treatment, indicated that there were no statistically significant differences between ^{177}Lu-PCTA-cetuximab-, single dose cetuximab-, and normal saline (control)-treated animals. However, at 4 weeks post-treatment, the ^{177}Lu-PCTA-cetuximab group showed statistically significantly lower values than

the other two (0.37 ± 0.12 vs. 1.06 ± 0.12 vs. 1.00 ± 0.09; $P < 0.05$).

SPECT/CT showed persistently high tumor uptake in the xenografts (Figure 5A, B). Thus, it is expected that the radioisotope particles delivered by cetuximab stay long enough to exert the therapeutic effects of particle emitting radiation after internalization.

Immunotherapy using tumor-targeted mAbs has experienced problems such as rapid tumor regrowth or the "rebound" radiographic phenomenon with accelerated clinical decline after cessation of maintenance treatment. We observed tumor regrowth over time in single-dose (100 μg) and multiple-dose (200 μg, 6 times /2weeks) cetuximab treatments. However, there was no tumor regrowth or rebound phenomenon in ^{177}Lu-PCTA-cetuximab treatment group. It was suggested that the radiation effect by radioisotopes inhibit the tumor regrowth or rebound phenomena.

In the present study, we focused on evaluating improved therapeutic effects of RIT using ^{177}Lu-PCTA-cetuximab compared to cetuximab-based immunotherapy alone. In future studies, the therapeutic efficacy of RIT for tumors that are resistant or less responsive to cetuximab or the combination therapeutic effect with cisplatin will be investigated.

Conclusions

Our results suggest that cetuximab can function as an effective carrier for tumor-targeted delivery of radiation, and that RIT using ^{177}Lu-PCTA-cetuximab is promising for targeted therapy of EGFR-positive tumors compared to antibody-based immunotherapy.

References

1. Forastiere AA, Goepfert H, Maor M, et al. Concurrent chemotherapy and radiotherapy for organ preservation in advanced laryngeal cancer. N Engl J Med 2003;349:2091–8.
2. Richey LM, Shores CG, George J, et al. The effectiveness of salvage surgery after the failure of primary concomitant chemoradiation in head and neck cancer. Otolaryngol Head Neck Surg 2007;136:98–103.
3. Argiris A, Stenson KM, Brockstein BE, et al. Neck dissection in the combined-modality therapy of patients with locoregionally advanced head and neck cancer. Head Neck 2004;26:447–55.
4. Schoder H, Fury M, Lee N, Kraus D. PET monitoring of therapy response in head and neck squamous cell carcinoma. J Nucl Med 2009;50 Suppl 1:74–88S.
5. Mendelsohn, J.; Baselga, J. Status of epidermal growth factor receptor antagonists in the biology and treatment of cancer. J. Clin. Oncol 2003;21: 2787−99.
6. Yarden Y, Sliwkowski MX. Untangling the ErbB signaling network. Nat Rev Mol Cell Biol 2001;2:127–37.

7. Grandis JR, Tweardy DJ. Elevated levels of transforming growth factor alpha and epidermal growth factor receptor messenger RNA are early markers of carcinogenesis in head and neck cancer. Cancer Res 1993;53:3579–84.
8. Bei R, Budillon A, Masuelli L, et al. Frequent overexpression of multiple ErbB receptors by head and neck squamous cell carcinoma contrasts with rare antibody immunity in patients. J Pathol 2004;204:317–25.
9. Ongkeko WM, Altuna X, Weisman RA, et al. Expression of protein tyrosine kinases in head and neck squamous cell carcinomas. Am J Clin Pathol 2005;124:71–6.
10. Normanno N, De Luca A, Bianco C, et al. Epidermal growth factor receptor (EGFR) signaling in cancer. Gene 2006;366:2–16.
11. Cohen EEW, Kane MA, List MA, et al. Phase II trial of gefitinib 250 mg daily in patients with recurrent and/or metastatic squamous cell carcinoma of the head and neck. Clin Cancer Res 2005;11:8418–24.
12. Soulieres D, Senzer NN, Vokes EE, et al. Multicenter phase II study of erlotinib, an oral epidermal growth factor receptor tyrosine kinase inhibitor, in patients with recurrent or metastatic squamous cell cancer of the head and neck. J Clin

Oncol 2004;22:77–85.

13. Vermorken JB, Trigo J, Hitt R, et al. Open-label, uncontrolled, multicenter phase II study to evaluate the efficacy and toxicity of cetuximab as a single agent in patients with recurrent and/or metastatic squamous cell carcinoma of the head and neck who failed to respond platinum-based therapy. J Clin Oncol 2007;25:2171–7.
14. Bernier J, Bentzen SM, Vermorken JB. Molecular therapy in head and neck oncology. Nat Rev Clin Oncol 2009;6:266–77.
15. Dittman K, Mayer C, Rodemann HP. Inhibition of radiation-induced of EGFR nuclear import by C225 (Cetuximab) suppresses DNA-PK activity. Radiother Oncol 2005;76:157–61.
16. Kang X, Patel D, Ng S, et al. High affinity Fc receptor binding and potent induction of antibody-dependent cellular cytotoxicity (ADCC) in vitro by anti- epidermal growth factor receptor antibody cetuximab. Proc Am Soc Clin Oncol 2007;25(18S). Abstract 3041.
17. Bonner JA, Harari PM, Giralt J, et al. Radiotherapy plus cetuximab for squamous cell carcinoma of the head and neck. N Engl J Med 2006;354:567–78.
18. Vermorken JB, Mesia R, Rivera F, et al. Platinum-based chemotherapy plus cetuximab in head and neck cancer. N Engl

J Med 2008;359:1116–27

19. Liu, Z.; Liu, Y.; Jia, B.; Zhao, H.; Jin, X.; Li, F.; Chen, X.; Wang, F. Epidermal growth factor receptor-targeted radioimmunotherapy of human head and neck cancer xenografts using 90Y-labeled fully human antibody panitumumab. Mol. Cancer Ther 2010;9: 2297−308.
20. Niu, G.; Sun, X.; Cao, Q.; Courter, D.; Koong, A.; Le, Q. T.; Gambhir, S. S.; Chen, X. Cetuximab-based immunotherapy and radioimmunotherapy of head and neck squamous cell carcinoma. Clin. Cancer Res 2010; 16: 2095−105.
21. Fischer, E.; Grunberg, J.; Cohrs, S.; Hohn, A.; Waldner-Knogler, K.; Jeger, S.; Zimmermann, K.; Novak-Hofer, I.; Schibli, R. L1-CAM- targeted antibody therapy and (177)Lu-radioimmunotherapy of disseminated ovarian cancer. Int. J. Cancer 2012;130: 2715−21.
22. Sharkey, R. M.; Goldenberg, D. M. Targeted therapy of cancer: new prospects for antibodies and immunoconjugates. Ca Cancer J. Clin 2006; 56: 226−43.
23. Bernhardt P, Forssell-Aronsson E, Jacobsson L, Skarnemark G. Low-energy electron emitters for targeted radiotherapy of small tumours. Acta Oncol 2001;40:602–8.

24. Bernhardt P, Benjegard SA, Kolby L, et al. Dosimetric comparison of radio- nuclides for therapy of somatostatin receptor-expressing tumors. Int J Radiat Oncol Biol Phys 2001;51:514–24.

25. Woo SK, Lee TS, Kim KM, et al. Anesthesia condition for ^{18}F-FDG imaging of lung metastasis tumors using small animal PET. *Nucl Med Biol*. 2008;35:143-50.

26. Park JJ, Lee TS, Son JJ, Chun KS, Song IH, Park YS, Kim KI, Lee YJ, Kang JH. Comparison of cell-labeling methods with ^{124}I-FIAU and ^{64}Cu-PTSM for cell tracking using chronic myelogenous leukemia cells expressing HSV1-tk and firefly luciferase. *Cancer Biother Radiopharm.* 2012;27:719-28.

27. Soulieres D, Senzer NN, Vokes EE, Hidalgo M, Agarwala SS, Siu LL. Multicenter phase II study of erlotinib, an oral epidermal growth factor receptor tyrosine kinase inhibitor, in patients with recurrent or metastatic squamous cell cancer of the head and neck. J Clin Oncol 2004;22:77–85..

28. Heimberger AB, Learn CA, Archer GE, et al. Brain tumors in mice are susceptible to blockade of epidermal growth factor receptor (EGFR) with the oral, specific, EGFR-tyrosine kinase inhibitor ZD1839 (iressa). Clin Cancer Res 2002;8:3496–502.

29. Hall, E.J. Radiobiology for the Radiologist. Philadelphia: J.B.

Lip- pincott Co., 1994.

30. Hernandez, M.C. and Knox, S.J. Radiobiology of radioimmunotherapy with Y-90 ibritumomab tiuxetan (Zevalin). Semin Oncol 2003;30:6-10.
31. Clynes, R.A.; Towers, T.L.; Presta, L.G.; Ravetch, J.V. Inhibitory Fc receptors modulate in vivo cytoxicity against tumor targets. Nat Med 2000; 6: 443-6.
32. Liu, Z.; Liu, Y.; Jia, B.; Zhao, H.; Jin, X.; Li, F.; Chen, X.; Wang, F. Epidermal growth factor receptor-targeted radioimmunotherapy of human head and neck cancer xenografts using 90Y-labeled fully human antibody panitumumab. Mol Cancer Ther 2010;9:2297−308.
33. Niu, G.; Sun, X.; Cao, Q.; Courter, D.; Koong, A.; Le, Q. T.; Gambhir, S. S.; Chen, X. Cetuximab-based immunotherapy and radioimmunotherapy of head and neck squamous cell carcinoma. Clin Cancer Res 2010;16:2095−105.
34. Huang, J.; Cui, L.; Wang, F.; Liu, Z. PET tracers based on (86)Y. Curr Radiopharm 2011; 4:122−30.
35. Nayak, T. K.; Brechbiel, M. W. 86Y based PET radiopharmaceuticals: radiochemistry and biological applications. Med Chem 2011;7:380−8.
36. Ferreira CL, Yapp DTT, Crisp S, et al. Comparison of

bifunctional chelates for 64Cu antibody imaging. Eur J Nucl Med Mol Imaging 2010;37:2117–26.

37. Chung CH, Ely K, McGavran L, et al. Increased epidermal growth factor receptor gene copy number is associated with poor prognosis in head and neck squamous cell carcinomas. J Clin Oncol 2006;24: 4170–6.
38. Rabinowits G, Haddad RI. Overcoming resistance to EGFR inhibitor in head and neck cancer: a review of the literature. Oral Oncol 2012 ;48(11):1085-9.
39. Sgouros, G. Dosimetry of internal emitters. J. Nucl. Med 2005; 46 (Suppl 1), 18S-27S.
40. Hatano K, Araki H, Sakai M, Kodama T, et al. Current status of intensity-modulated radiation therapy (IMRT). Int J Clin Oncol 2007; 12: 408-15.
41. Green N, Kern W. Clinical Course and Treatment Results of Patients with Postresection Locally Recurrent Lung-Cancer. Cancer 1978; 42: 2478-82.
42. Laperriere N, Zuraw L, Cairncross G. Radiotherapy for newly diagnosed malignant glioma in adults: a systematic review. Radiother Oncol 2002; 64: 259-73.
43. Plataniotis GA, Dale RG. Biologically Effective Dose-Response Relationship for Breast Cancer Treated by

Conservative Surgery and Postoperative Radiotherapy. Int J Radiat Oncol Biol Phys 2009; 75: 512-17.

44. Dawson LA, Lawrence TS. The role of radiotherapy in the treatment of liver metastases. Cancer J 2004; 10: 139-44.
45. Miller RC, Iott MJ, Corsini MM. Review of Adjuvant Radiochemotherapy for Resected Pancreatic Cancer and Results from Mayo Clinic for the 5Th Jucts Symposium. Int J Radiat Oncol Biol Phys 2009; 75: 364-68.
46. Tempero M, Leichner P, Baranowska-Kortylewicz J et al. High-dose therapy with (90)yttrium-labeled monoclonal antibody CC49: A phase I trial. Clin Cancer Res 2000; 6: 3095-102.

Table 1. Biodistribution of ^{177}Lu-PCTA-cetuximab in SNU-1066 tumor-bearing mice.

	2 h	day 1	day 3	day 5	day 7	day 7 (blocking)	day 14
Blood	29.0±3.6	13.0±2.0	8.2±1.9	5.8±2.0	3.8±1.3	2.4±0.9	2.3±0.4
Heart	5.9±0.8	3.7±0.3	2.6±0.4	2.0±0.6	1.5±0.2	1.2±0.3	1.0±0.1
Liver	23.2±1.9	22.9±5.2	16.1±3.9	9.9±1.9	8.3±1.0	12.9±2.6	5.7±0.8
Lung	9.4±2.6	5.7±0.4	3.5±1.3	2.7±0.7	2.9±0.3	1.7±0.3	1.9±0.3
Spleen	9.0±3.1	9.3±2.6	10.3±6.8	8.9±4.7	7.9±1.2	3.5±0.7	7.9±1.4
Kidney	10.1±1.2	6.4±0.9	3.7±0.2	3.0±0.3	2.9±0.2	2.0±0.3	1.7±0.2
Stomach	1.3±0.4	2.0±0.4	1.0±0.4	0.9±0.2	0.9±0.2	0.4±0.1	0.5±0.1
S.I.*	3.2±0.6	2.4±0.3	1.5±0.3	1.2±0.3	1.0±0.1	0.5±0.1	0.6±0.1
L.I.**	1.8±0.4	3.1±0.7	1.8±0.3	1.1±0.3	0.9±0.1	0.8±0.3	0.6±0.1
Muscle	1.1±0.1	2.2±0.1	1.4±0.3	1.0±0.4	0.9±0.1	0.5±0.1	0.5±0.1
Femur	2.3±0.1	4.3±0.8	6.3±1.0	6.3±0.7	6.5±0.3	3.5±1.3	7.6±1.0
SNU-1066	2.5±0.6	11.4±2.6	16.2±4.9	16.8±2.6	20.6±5.2	5.4±3.0	17.5±4.9
T/B†	0.1±0.0	0.9±0.1	2.0±0.5	3.1±1.0	6.3±3.8	2.3±1.0	7.7±2.6
T/M††	2.3±0.7	5.1±1.0	11.7±1.4	19.4±8.2	21.9±2.7	9.7±4.0	36.4±13.1
T/L†††	0.1±0.0	0.5±0.2	1.1±0.6	1.8±0.5	2.4±0.3	3.0±1.4	3.1±0.7

*; Small intestine; **, Large intestine

†, Tumor-to-Blood ratio; ††, Tumor-to-Muscle ratio; †††, Tumor-to-Liver ratio.

Table 2. Extrapolated radiation dosimetry to an adult human after intravenous injection of ^{177}Lu-PCTA-cetuximab based on the biodistribution data obtained form SNU-1066 tumor-bearing mice.

Organ	mGy/MBq	rad/mCi
Adrenals	$7.3 \times 10^{-5} \pm 4.6 \times 10^{-6}$	$2.7 \times 10^{-4} \pm 1.7 \times 10^{-5}$
Brain	$2.9 \times 10^{-7} \pm 1.8 \times 10^{-7}$	$1.1 \times 10^{-5} \pm 6.6 \times 10^{-6}$
Breasts	$2.9 \times 10^{-4} \pm 1.5 \times 10^{-5}$	$1.1 \times 10^{-3} \pm 5.5 \times 10^{-5}$
LLI*	$2.8 \times 10^{-3} \pm 1.8 \times 10^{-3}$	$1.0 \times 10^{-2} \pm 6.6 \times 10^{-3}$
Small Intestine	$5.5 \times 10^{-4} \pm 3.5 \times 10^{-4}$	$2.0 \times 10^{-3} \pm 1.3 \times 10^{-3}$
Stomach Wall	$3.7 \times 10^{-3} \pm 8.6 \times 10^{-4}$	$1.4 \times 10^{-2} \pm 3.2 \times 10^{-3}$
ULI**	$2.9 \times 10^{-5} \pm 5.1 \times 10^{-6}$	$1.1 \times 10^{-4} \pm 1.9 \times 10^{-5}$
Kidneys	$5.7 \times 10^{-3} \pm 3.1 \times 10^{-4}$	$2.1 \times 10^{-2} \pm 1.2 \times 10^{-3}$
Liver	$6.0 \times 10^{-2} \pm 4.5 \times 10^{-3}$	$2.2 \times 10^{-1} \pm 1.7 \times 10^{-2}$
Lungs	$7.7 \times 10^{-2} \pm 6.1 \times 10^{-3}$	$2.9 \times 10^{-1} \pm 2.3 \times 10^{-2}$
Muscle	$1.6 \times 10^{-5} \pm 1.2 \times 10^{-6}$	$5.8 \times 10^{-5} \pm 4.4 \times 10^{-6}$
Ovaries	$8.6 \times 10^{-4} \pm 2.8 \times 10^{-4}$	$3.2 \times 10^{-3} \pm 1.0 \times 10^{-3}$
Pancreas	$1.1 \times 10^{-4} \pm 9.6 \times 10^{-6}$	$3.9 \times 10^{-4} \pm 3.6 \times 10^{-5}$
Red Marrow	$8.2 \times 10^{-4} \pm 6.5 \times 10^{-5}$	$3.0 \times 10^{-3} \pm 2.4 \times 10^{-4}$
Osteogenic Cells	$8.3 \times 10^{-5} \pm 5.8 \times 10^{-6}$	$3.1 \times 10^{-4} \pm 2.2 \times 10^{-5}$
Skin	$2.5 \times 10^{-5} \pm 1.7 \times 10^{-6}$	$9.3 \times 10^{-5} \pm 6.2 \times 10^{-6}$
Spleen	$2.3 \times 10^{-1} \pm 3.1 \times 10^{-2}$	$8.7 \times 10^{-1} \pm 1.2 \times 10^{-1}$
Thymus	$1.9 \times 10^{-5} \pm 7.9 \times 10^{-7}$	$1.1 \times 10^{-4} \pm 4.3 \times 10^{-5}$
Thyroid	$6.3 \times 10^{-5} \pm 3.8 \times 10^{-6}$	$7.2 \times 10^{-5} \pm 2.9 \times 10^{-6}$
Urinary Bladder Wall	$5.8 \times 10^{-5} \pm 1.6 \times 10^{-5}$	$2.1 \times 10^{-4} \pm 1.4 \times 10^{-5}$
Uterus	$9.9 \times 10^{-6} \pm 2.2 \times 10^{-6}$	$3.4 \times 10^{-5} \pm 1.1 \times 10^{-5}$
Effective Dose	3.3×10^{-1}	1.4×10^{0}
SNU-1066 tumor	$6.5 \times 10^{3} \pm 3.0 \times 10^{3}$	$2.4 \times 10^{4} \pm 1.1 \times 10^{4}$

Data were presented as mean ± S.D. (n=3 or 4)

*, lower large intestine, **, upper large intestine

Figure Legends

Fig. 1. **Characterization of EGFR expression in head and neck squamous cell carcinoma (HNSCC) cells.** (A) Expression of EGFR in HNSCC cells by RT-PCR and protein level by Western blot. (B) Flow cytometry in HNSCC cells. (C) The anti-growth effect of cetuximab in YD-8, SNU-1041, SNU-1071 and SNU-1066 HNSCC cells exposed to different concentration cetuximab at 72h. The viability of SNU1066 cells treated with cetuximab decreased in a dose dependent manner, as evaluated by the MTS assay.

Fig. 2. **Cell binding assay and cell viability assay of ^{177}Lu-PCTA-cetuximab in HNSCC cell lines.** (A) Quantitative cellular binding of ^{177}Lu-PCTA-cetuximab to YD-8, SNU-1041, SNU-1071 and SNU-1066 cell lines was compared with each other. Data were presented as mean ± S.D. (n = 3). (B) Cytotoxicity of ^{177}Lu-PCTA-cetuximab in SNU-1066 cells. (C) ^{177}Lu-PCTA-cetuximab-induced activation of EGFR and of downstream signaling pathways mediated by Akt or Erk.

Fig. 3. **Characteristics of ^{177}Lu-PCTA-cetuximab.** (A) MALDI mass spectra of cetuximab and PCTA-cetuximab. The PCTA coupling

distribution was estimated from relative peak intensities of the mass. (B) ITLC radiochromatograms of ^{177}Lu-PCTA-cetuximab. Radiolabeling yield of the radioimmunoconjugates was > 98%.

Fig. 4. **Biodistribution of ^{177}Lu-PCTA-cetuximab in SNU-1066 tumor-bearing mice.** ^{177}Lu-PCTA-cetuximab (100 μg/3.7 MBq) was injected intravenously into mice. For each time point, the mice were sacrificed and the percentage of the injected radioactivity dose/gram (%ID/g) was determined. Data were presented as mean ± S.D. (n = 4). S.I., small intestine; L.I., large intestine.

Fig. 5. **Micro-SPECT/CT images of ^{177}Lu-PCTA-cetuximab in SNU-1066 tumor-bearing mice.** At 5 days (A) post-injection of ^{177}Lu-PCTA-cetuximab (350 μCi/100 μg/0.1 mL), a SPECT/CT volume image and coronal images were acquired for 120 min with small animal SPECT/CT system (Bioscan). Immediately after SPECT/CT acquisition, frozen and whole body sections and autoradiographic images were obtained using BAS-5000. Frozen section photo images (C) and digital whole body autoradiographic images (D) were obtained from the same mouse. For blocking study, SPECT/CT volume image (E) and coronal images (F) were acquired from mice administrated with excess

cetuximab prior to ^{177}Lu-PCTA-cetuximab injection. Tumors are indicated by white dotted circles.

Fig. 6. **Radioimmunotherpeutic efficacy of ^{177}Lu-PCTA-cetuximab in SNU-1066 tumor-bearing mice.** The treatment was initiated on day 0. Tumor growth in SNU-1066 tumor-bearing mice treated with saline, cetuximab (single or multiple-dose) and ^{177}Lu-PCTA-cetuximab were as compared to each other. SNU-1066 tumor growth was inhibited by ^{177}Lu-PCTA-cetuximab treatment, but tumor growth persisted continuously in other groups. Data represents mean tumor volumes ± S.D.*= vs. saline-treated group, **= vs. single dose group, †= vs. multiple dose group; $P < 0.05$.

Fig. 7. **Body weight changes in SNU-1066 tumor-bearing mice administered saline, cetuximab, or ^{177}Lu-PCTA-cetuximab.** Body weight was monitored three times a week during therapy. No significant weight loss was observed in saline, cetuximab (single- or multiple-dose), and ^{177}Lu-PCTA-cetuximab treatment groups, indicating that radioimmunotherapy using ^{177}Lu-PCTA-cetuximab was well tolerated.

Fig. 8. **Monitoring of the therapeutic response of ^{177}Lu-PCTA-**

cetuximab using ^{18}F-FDG-PET imaging in SNU-1066 tumor-bearing mice. ^{18}F-FDG-PET images were obtained before treatment and at 1, 2, and 4 weeks after treatment with either saline, cetuximab (5 mg/kg, single dose) or ^{177}Lu-PCTA-cetuximab (12.95 MBq, single dose) (A). Tumors are indicated by white dotted circles. Tumor uptake of ^{18}F-FDG was quantified from small animal PET scans (n = 3) and represented as SUV (B). ^{177}Lu-PCTA-cetuximab treatment group showed a marked reduction in FDG SUV, compared with other groups. *; $P < 0.05$.

Fig. 9. **Immunohistochemistry and TUNEL assay in SNU-1066 tumors.** Quantity of Ki-67-positive cells were markedly decreased in ^{177}Lu-PCTA-cetuximab treatment xenograft tumor tissues in comparison with the saline and cetuximab treatment groups (A and C). There were statistically significant differences in apoptosis levels among ^{177}Lu-PCTA-cetuximab, saline and cetuximab treatment groups as determined by TUNEL assay (A and B). * $P<0.01$.

Figures

Figure 1.

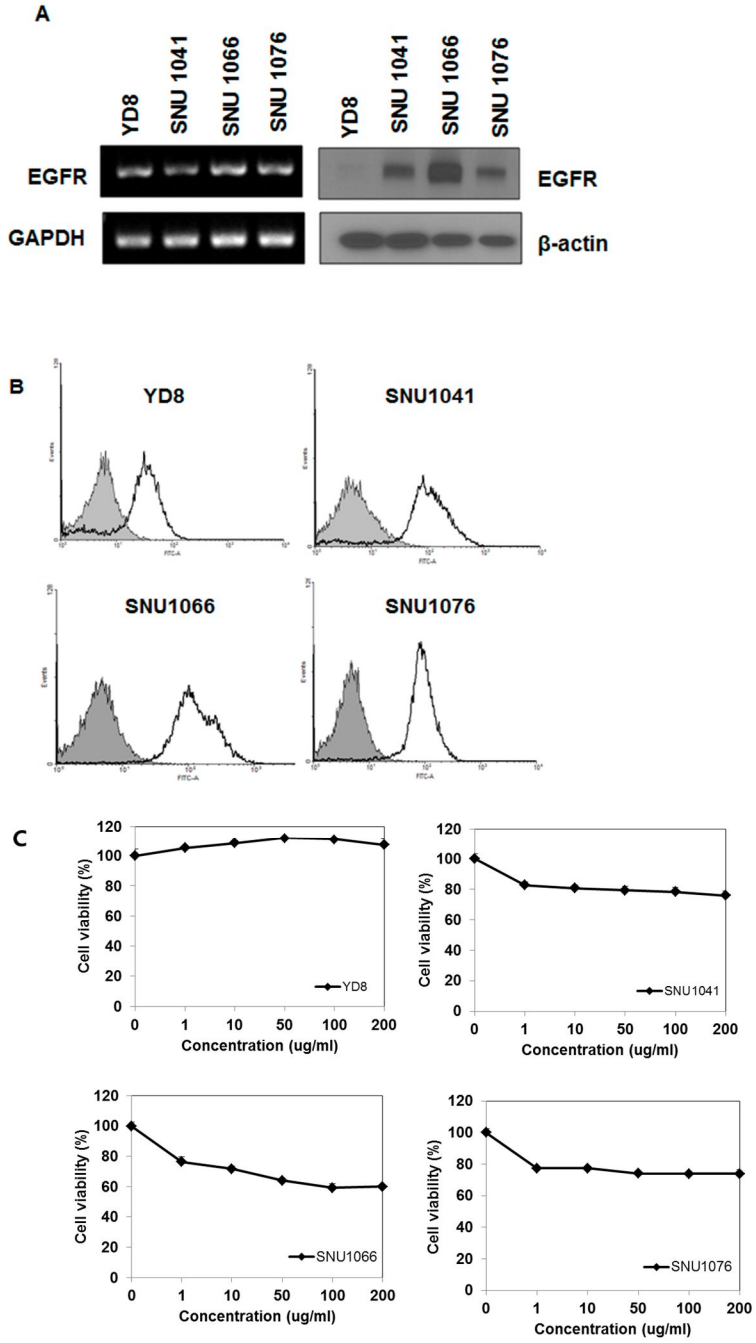

Figure 2.

A

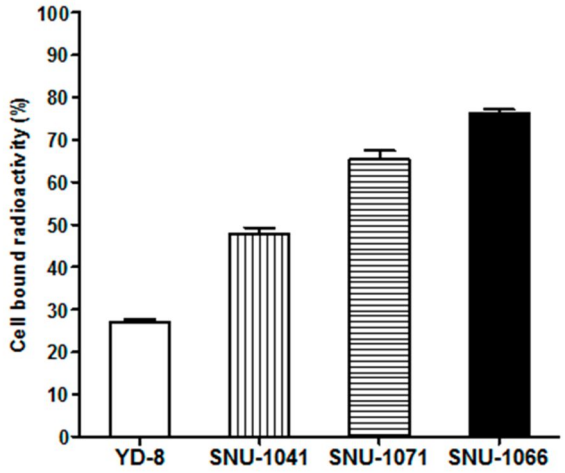

B

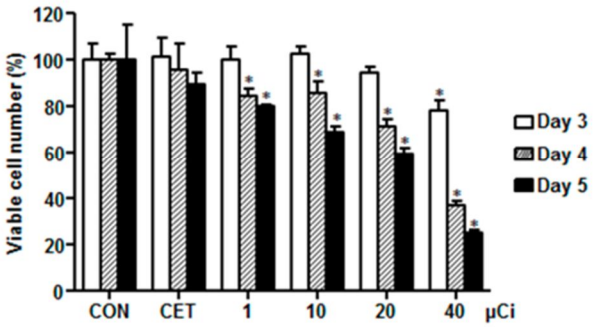

CON; control
CET; cold cetuximab treatment
*; vs. control of each time point, $P < 0.05$

C

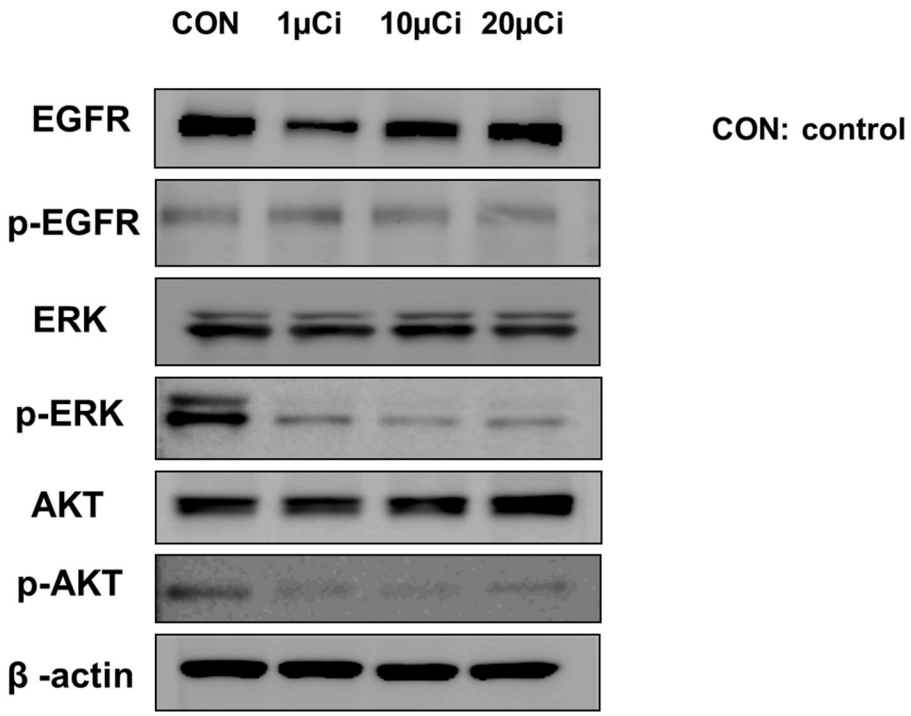
CON
1μCi
10μCi
20μCi
EGFR
p-EGFR
ERK
p-ERK
AKT
p-AKT
β -actin
CON: control

Figure 3.

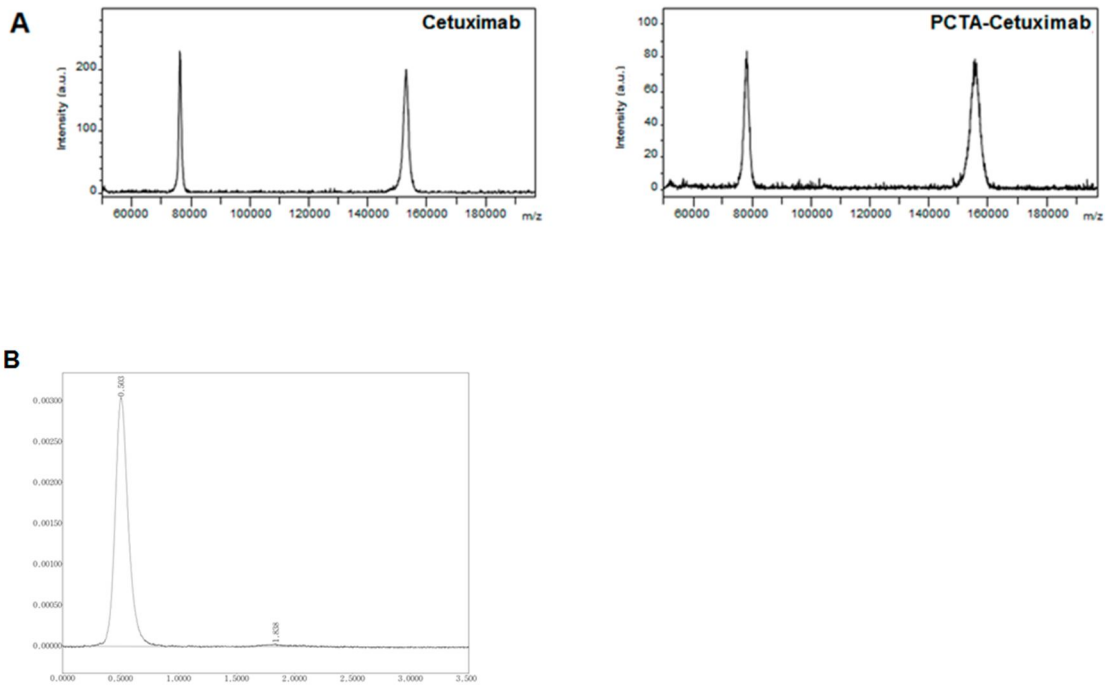
A
Cetuximab
Intensity (a.u.)
m/z
PCTA-Cetuximab
Intensity (a.u.)
m/z
B

Figure 4.

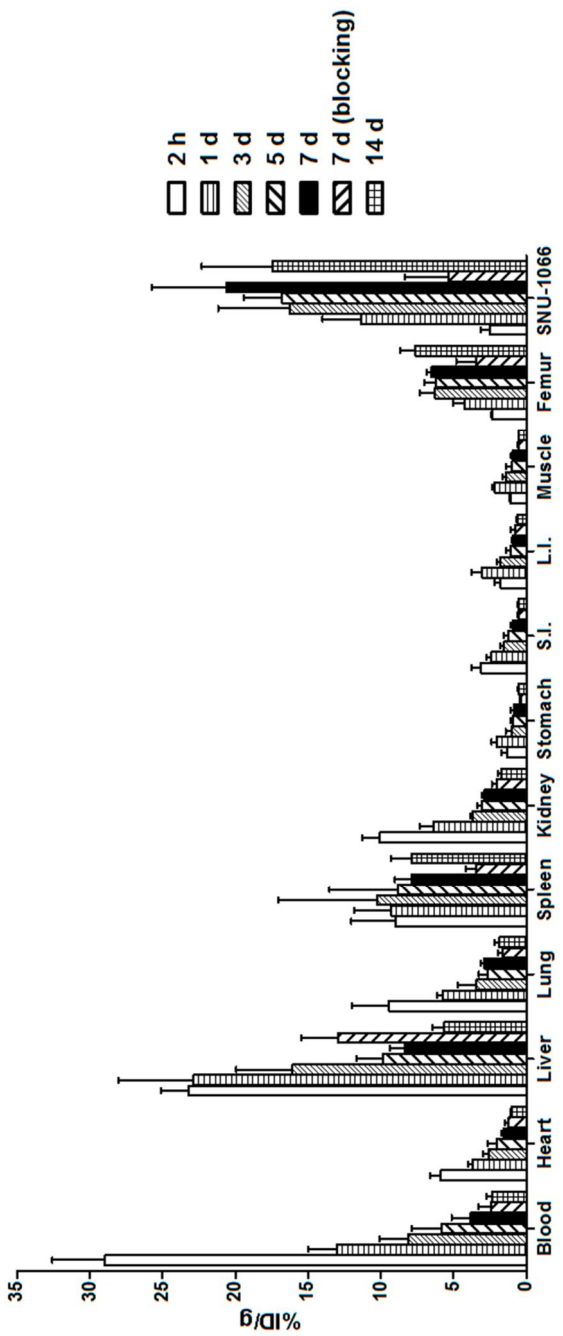
2 h
1 d
3 d
5 d
7 d
7 d (blocking)
14 d
%ID/g
0
5
10
15
20
25
30
35
Blood
Heart
Liver
Lung
Spleen
Kidney
Stomach
S.I.
L.I.
Muscle
Femur
SNU-1066

Figure 5.

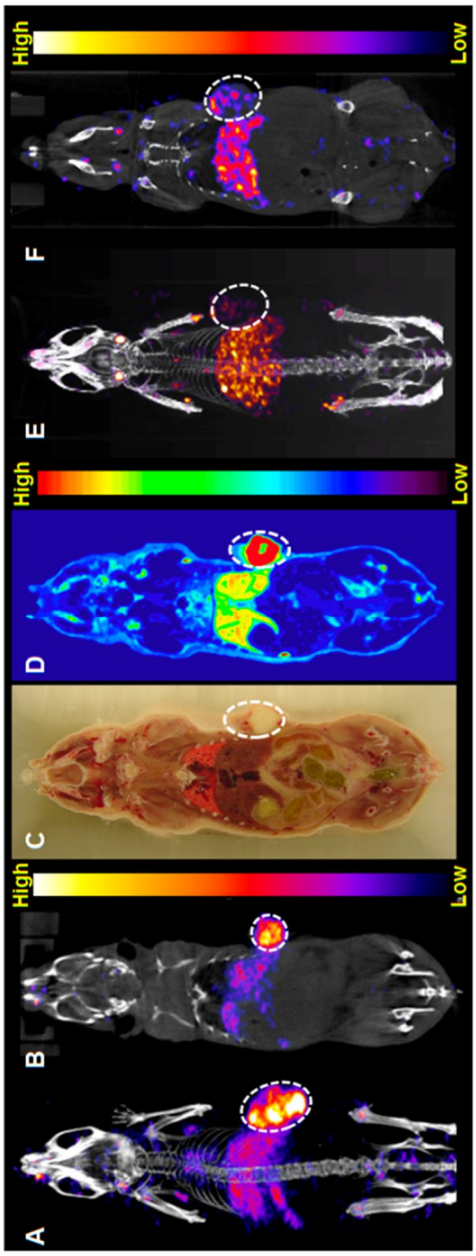

Figure 6.

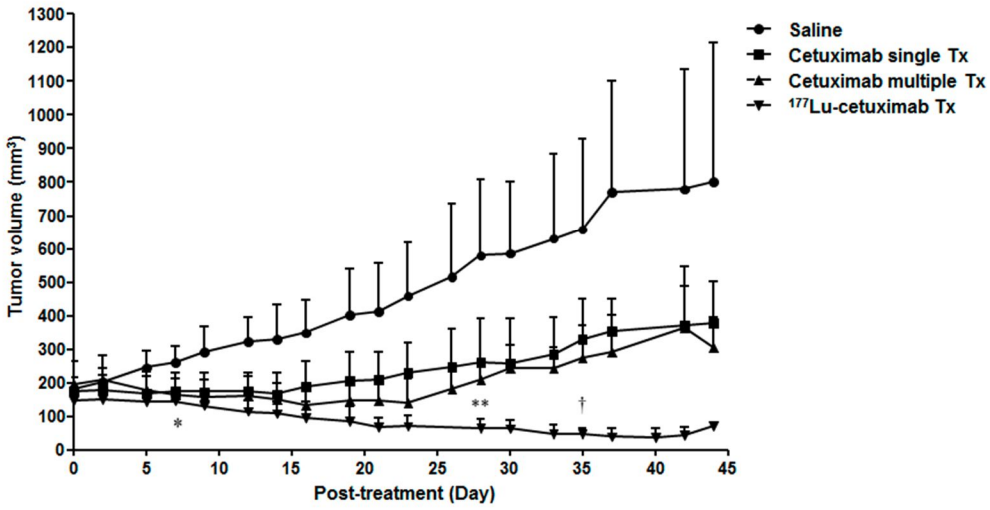
Saline
Cetuximab single Tx
Cetuximab multiple Tx
177Lu-cetuximab Tx
Tumor volume (mm3)
Post-treatment (Day)
1300
1200
1100
1000
900
800
700
600
500
400
300
200
100
0
0
5
10
15
20
25
30
35
40
45
*
**
†

Figure 7.

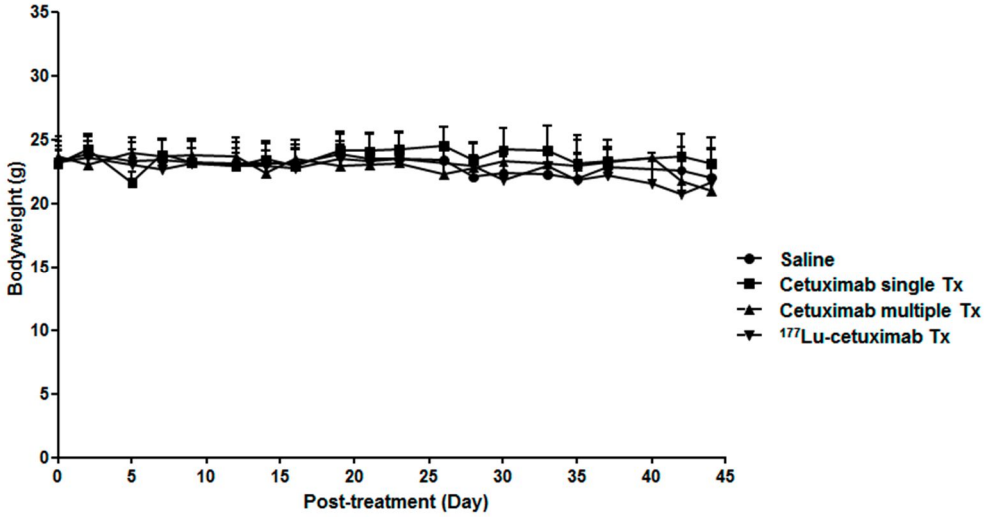
Bodyweight (g)
35
30
25
20
15
10
5
0
0
5
10
15
20
25
30
35
40
45
Post-treatment (Day)
Saline
Cetuximab single Tx
Cetuximab multiple Tx
177Lu-cetuximab Tx

Figure 8.

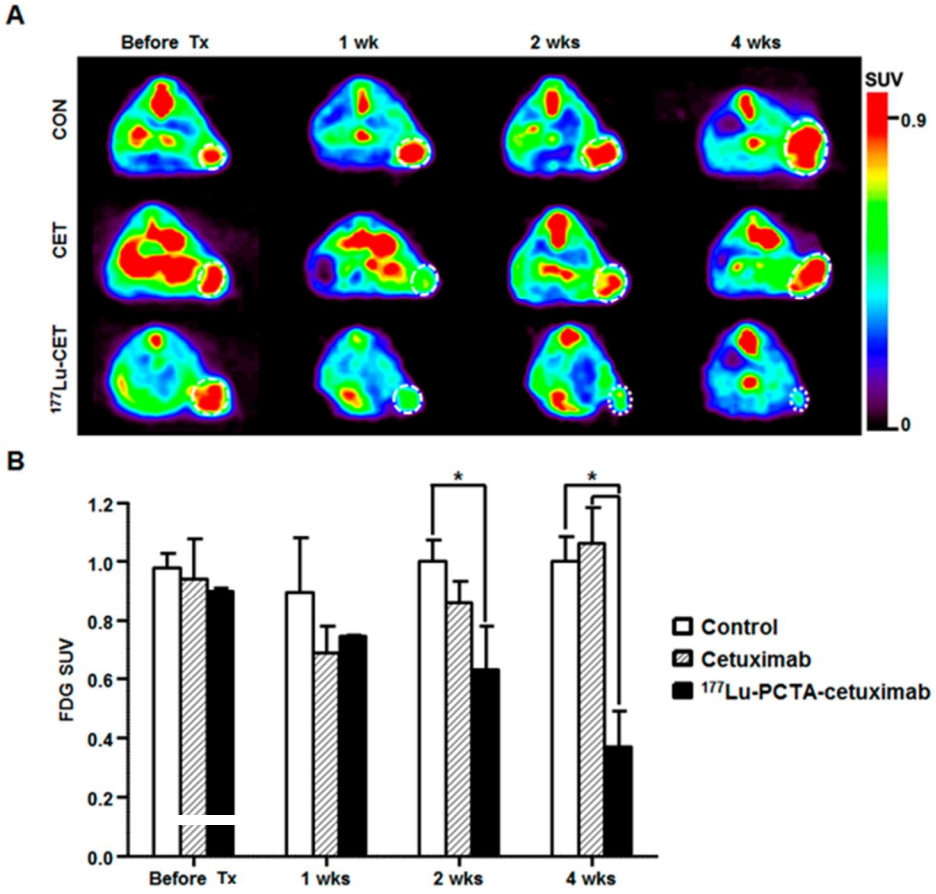
A
Before Tx
1 wk
2 wks
4 wks
CON
CET
177Lu-CET
SUV
0.9
0
B
FDG SUV
1.2
1.0
0.8
0.6
0.4
0.2
0.0
Before Tx
1 wks
2 wks
4 wks
*
*
Control
Cetuximab
177Lu-PCTA-cetuximab

Figure 9.

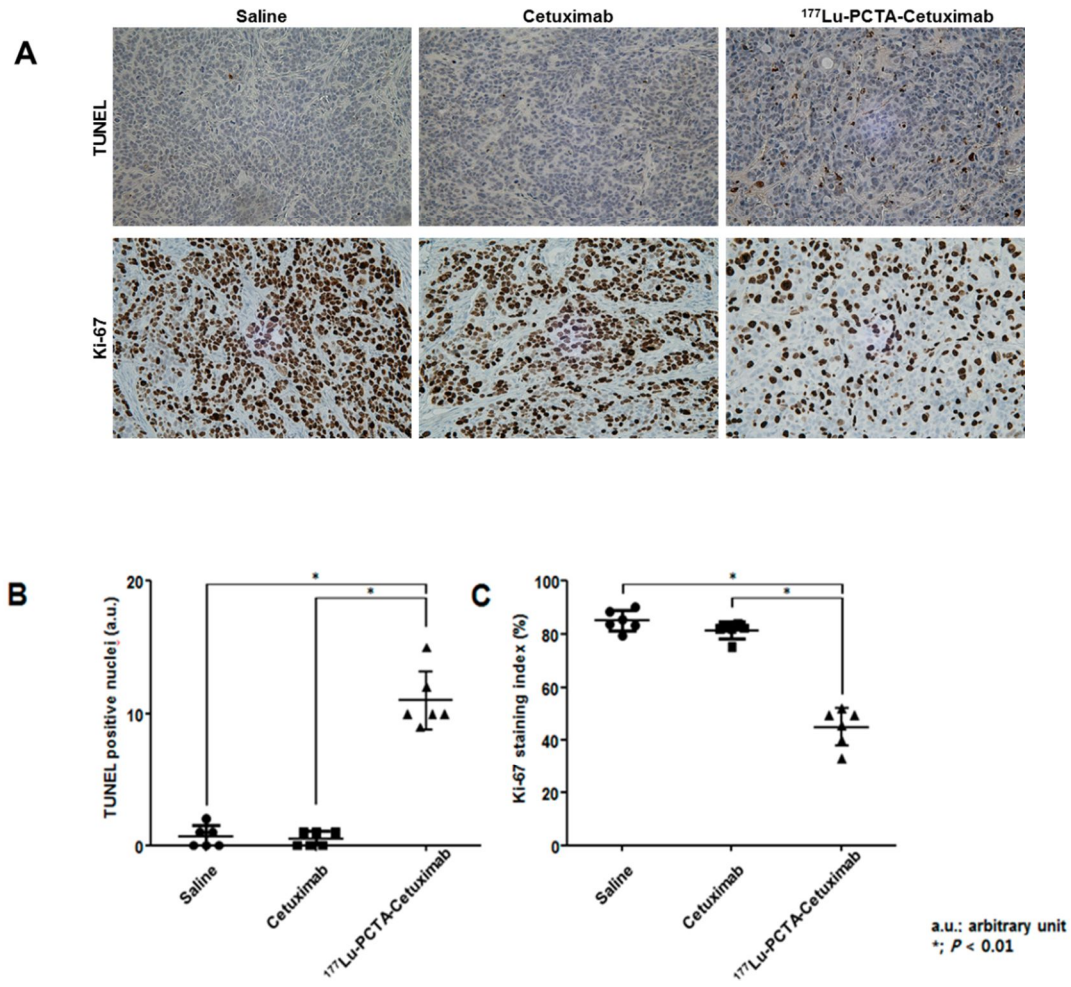
A
Saline
Cetuximab
177Lu-PCTA-Cetuximab
TUNEL
Ki-67
B
TUNEL positive nuclei (a.u.)
20
10
0
*
*
Saline
Cetuximab
177Lu-PCTA-Cetuximab
C
Ki-67 staining index (%)
100
80
60
40
20
0
*
*
Saline
Cetuximab
177Lu-PCTA-Cetuximab
a.u.: arbitrary unit
*; P < 0.01

국문초록

배경: 임상적으로 EGFR 발현 두경부암에 대해서 항 EGFR 단일클론 항체를 이용한 다양한 항암치료가 시도되고 있지만 여러가지 저항 기전으로 인하여 뛰어난 치료효과를 보여주지 못하고 있다. 본 연구에서는 항 EGFR 단일클론 항체 단독치료의 제한점을 극복하기 위한 치료방법으로 ^{177}Lu 표지 항-EGFR 단일클론항체를 이용한 방사면역치료의 효과를 EGFR 발현 두경부암 생쥐모델을 통해서 확인해보고자 한다.

방법:

1. ^{177}Lu-PCTA-cetuximab 표지

^{177}Lu을 cetuximab 항체에 표지하기 위하여 PCTA가 접합된 cetuximab을 제조하였으며, 2 mg/mL의 농도로 준비하였다. PCTA 접합 cetuximab을 1.5 mL microcentrifuge tube에 준비하고, ^{177}Lu을 tube 첨가한 뒤 thermomixer를 이용하여 37℃에서 60분 간 ^{177}Lu 방사표지반응을 진행하였다.

2. 두경부암 모델에서 ^{177}Lu 표지 항-EGFR 항체의 생체내분포 실험 및 Micro-SPECT/CT 영상

두경부암 세포주인 SNU-1066를 배양하여 1.2 × 10^7 개를 150 μL의 PBS로 희석하여 BALB/c athymic female 마우스의 우측 옆구리 피하에 주사하였다. 100 mm^3~ 200 mm^3 사이가 되었을 때 ^{177}Lu-PCTA-cetuximab 3.7 MBq 를 꼬리정맥에 정주하고 14일까지 생체내분포를 측정하였다. SNU-1066 종양모델에서 5일째 ^{177}Lu-PCTA-cetuximab (12.95 MBq)을 정주하고 Micro-SPECT/CT를 시행하였다. ^{177}Lu-PCTA-cetuximab를 정주하기 30분전에 cetuximab (40 mg/kg mouse body weight)를 정주하여 차단실험을 하였다

3. 치료용 동위원소 ^{177}Lu 표지 항-EGFR 항체의 방사면역치료 평가

1) 두경부암 모델에서 ^{177}Lu 표지 항-EGFR 항체의 치료효과

두경부암 세포주인 SNU-1066를 배양하여 1.2 × 10^7 개를 150 μL의 PBS로 희석하여 BALB/c athymic female 마우스의 우측 옆구리 피하에 주사하였다. 종양의 크기가 100 mm^3~ 200 mm^3 사이가 되었을 때, 대조군과 cetuximab 단회투여군 (single tx.), cetuximab 반복투여군 (multiple tx.), ^{177}Lu-PCTA-cetuximab 투여군으로 실험군을 선정하고 치료를 시작하였다. 각 군 당 9~10 마리의 SNU-1066 두경부암 모델을 이용하여 분석하였으며, 대조군은 생리식염수 100 μL, 치료군에서 cetuximab 단회투여군은 cetuximab 5 mg/kg (마리 당 100 μg), cetuximab 반복투여군은 cetuximab 10 mg/kg (마리 당 200 μg)을 주 3회 2주 (총 6회), ^{177}Lu-PCTA-cetuximab 투여군은

^{177}Lu 표지 cetuximab 12.95 MBq를 꼬리 정맥을 통해 주사하였다. 주 3회 종양의 크기와 마우스의 몸무게를 측정하였으며, 치료 전, 치료 시작 후 1주, 2주, 4주에 각 군 당 3마리의 모델을 이용하여 FDG-PET 영상을 획득하였다. (cetuximab 반복투여군 제외).

2) 두경부암 모델에서 ^{177}Lu 표지 항-EGFR 항체의 치료효과 모니터링 (FDG-PET) 영상

SNU-1066 두경부암 모델을 생리식염수 투여군, cetuximab 단회투여군, cetuximab 반복투여군, ^{177}Lu-PCTA-cetuximab 투여군으로 나누어 치료하는 과정에서 치료효과에 따른 포도당 대사의 차이를 평가하고 종양 치료에 대한 반응을 확인하고자 치료 전, 치료 시작 후 1주, 2주, 4주에 각 군별 3마리 모델을 2% isofluorane를 이용한 호흡 마취 하에서 FDG 200 μCi를 꼬리정맥을 통해 주사하고, 주사 후 1시간 뒤 소동물 PET 영상장비(microPET R4 PET scanner)를 이용하여 20분간 정적영상을 획득하였다. 획득한 영상은 ASIpro 프로그램을 이용하여 분석하여 SUV(Standardized Uptake Value) 영상으로 나타내어 종양의 ROI(region of interest) 분석을 실시하여 비교 평가하였다.

결과:

1. ^{177}Lu-PCTA-cetuximab 표지

반응 후 간이박층크로마토그래피 (instant thin chromatography, ITLC)를 이용하여 방사표지수율을 계산하였으며, 이 때의 방사표지수율은 98.20%였다.

2. 두경부암 모델에서 ^{177}Lu 표지 항-EGFR 항체의 생체내분포 실험 및 Micro-SPECT/CT 영상

생체내분포도 실험에서 ^{177}Lu-PCTA-cetuximab 은 다른 장기에서는 시간이 지나감에 따라서 활성도가 감소하는 것에 반해서 SNU-1066 두경부암 종양에서는 7일째 20.6 ± 5.2%ID/g까지 활성도가 증가하다가 14일째까지는 17.5 ± 4.9 %ID/g으로 서서히 감소하였다. cetuximab으로 미리 차단을 한 경우에는 7일째 ^{177}Lu-PCTA-cetuximab의 섭취율이 26.0%까지 감소하였다. ^{177}Lu-PCTA-cetuximab 정주 이후 5일째 얻은 Micro-SPECT/CT 영상에서는 SNU-1066 두경부암 종양에서는 뚜렷하게 섭취된 것을 확인할 수 있었고 cetuximab으로 미리 차단을 한 경우에는 섭취율이 급격하게 감소함을 확인하였다.

3. 치료용 동위원소 ^{177}Lu 표지 항-EGFR 항체의 방사면역치료 평가

1) 두경부암 모델에서 ^{177}Lu 표지 항-EGFR 항체의 치료효과

대조군에서 SNU-1066 종양이 지속적으로 성장하였으며, cetuximab 단회치료군은 치료 후 14일까지 종양의 성장이 억제되었으나 이후

계속적으로 성장하였다. cetuximab 반복투여군은 치료 후 16일까지 종양의 크기가 감소하는 경향을 보였으나 이후 종양의 성장이 지속적으로 증가하였다. ^{177}Lu-cetuximab 투여군에서는 치료 후 종양의 크기는 지속적으로 감소하였으며, 대조군과는 치료 후 9일부터, cetuximab 단회투여군과는 치료 후 21일부터, cetuximab 반복투여군과는 치료 후 35일째부터 통계적으로 유의한 차이를 보였다. ($p < 0.05$). cetuximab 반복투여군은 반복치료에도 불구하고 cetuximab 단회투여군과 통계적으로 유의한 차이를 보이지 않았다.

2) 두경부암 모델에서 ^{177}Lu 표지 항-EGFR 항체의 치료효과 모니터링 (FDG-PET) 영상

FDG-PET의 SUV(standard uptake values) 영상에서 종양의 ROI(region of interest) 분석을 실시하여 비교 평가한 결과, FDG-PET의 SUV는 ^{177}Lu-cetuximab 투여군, cetuximab 단회투여군, 대조군 각각 치료전 (0.90 ± 0.01 vs 0.94 ± 0.14 vs 0.94 ± 0.05; $P=0.89$), 치료 1주차 (0.74 ± 0.01 vs $0.69\pm0.0.09$ vs 0.90 ± 0.18; $P=0.69$), 치료 2주차 (0.63 ± 0.15 vs 0.86 ± 0.08 vs 1.00 ± 0.07; $P=0.105$)에는 통계학적으로 유의한 차이가 없었으나 치료 4주차 (0.37 ± 0.12 vs 1.06 ± 0.12 vs 1.00 ± 0.09; $P < 0.05$) 에는 통계적으로 유의한 감소를 보였다.

결론: 본 연구에서는 EGFR 발현 두경부암 생쥐 모델에서 ^{177}Lu 표지 항EGFR 단일클론 항체를 이용한 방사면역치료가 단일클론항체 단독 면역치료에 비해서 통계학적으로 유의하게 높은 항암치료효과를 확인하였다.

주요어: 방사면역치료, 방사성동위원소, 단일클론항체, 표피성장인자수용체, 두경부, 편평상피세포암

학 번: 2010-31149